# Molecular Diffusion and Photooxidation Chemistry on $TiO_2$ Surfaces under Perfluoroalkane Layers

**D. Panayotov* and J. T. Yates, Jr.**

*Department of Chemistry, Surface Science Center, University of Pittsburgh, Pittsburgh, Pennsylvania 15260*

*Received: October 16, 2003*

The photooxidation of an organic compound, 2-chloroethyl ethyl sulfide (2-CEES), over a $TiO_2-SiO_2$ mixed oxide photocatalyst has been studied using transmission infrared spectroscopy. The purpose of this work was to determine the influence of an inert perfluoroalkane buffer layer on the photooxidation properties of the photocatalyst. Both oxygen gas and 2-CEES were adsorbed on top of a thick $C_9F_{20}$ layer, and it was found that the diffusion of both of the reactants through the solid perfluoroalkane layer occurs readily at 253 K. Adsorption of 2-CEES and $O_2$ therefore occurs at the photocatalyst surface, and photooxidation of the 2-CEES is little impeded by the inert $C_9F_{20}$ layer. Both $C_9F_{20}$ and 2-CEES cause characteristic frequency shifts due to hydrogen bonding with Si−OH groups on the photocatalyst, and this effect may be used spectroscopically to monitor the displacement of hydrogen-bonded $C_9F_{20}$ molecules from the Si−OH groups by the 2-CEES molecule. In addition, IR spectroscopy has been used to monitor the diffusion of oxygen gas through the perfluoroalkane layer, and it has been found that $O_2$ diffusion occurs at 253 K.

## I. Introduction

The photooxidation of organic molecules over $TiO_2$-based photocatalysts is of importance in environmental cleanup[1−4] and is becoming widely used technologically.[5,6] In most cases, this method leads to the complete mineralization of organic molecules to $CO_2$, $H_2O$, and inorganic salts without forming hazardous final byproducts. The $TiO_2$-mediated photooxidation is also attracting attention as a method for the degradation of chemical warfare agents (CWAs). Recently, the $TiO_2$-mediated photooxidation of mustard gas simulants, diethyl sulfide (DES),[7,8] and 2-chloroethyl ethyl sulfide (2-CEES)[9,10] has been reported.

The heterogeneous photocatalytic oxidation of organic molecules often obeys a Langmuir−Hinshelwood (LH)-type mechanism, and site blocking by oxidation product species could be expected. The activity of the mixed oxide photocatalyst, $TiO_2-SiO_2$, is reported to exceed that of pure $TiO_2$ powders.[11,12,13] The advantage of the $TiO_2-SiO_2$-based photocatalysts is that they may combine the photoactivity of $TiO_2$ with the adsorptive properties of the high surface area $SiO_2$ phase.[11−13] We have shown previously[14] that Si−OH groups present on the partially dehydroxylated $TiO_2-SiO_2$ powder act as anchor groups for hydrogen-bonding electrophilic molecules, holding them near the $TiO_2$ sites that are then able to photocatalyze their oxidation.

Fluorinated compounds can be used as coating films for different substrates or as a phase-separation layer. Because the fluorocarbon chains have weak interactions among themselves, it is difficult to deposit fluoroalkanes on a solid substrate in multilayer form. In the case of fluoroalkane adsorption on the surface of $TiO_2-SiO_2$, the driving forces may be the $F\cdots O_{surface}$ van der Waals interaction together with the formation of H bonds with surface silanol groups, $Si-OH\cdots F$.

This work has probed the role of a thick layer of a perfluoroalkane, $C_9F_{20}$, in the transport of 2-CEES and $O_2$ to the photocatalyst surface at 253 K, which is slightly below the melting point of $C_9F_{20}$ (mp = 257 K [15]). It is believed that the experiment provides a model for the behavior of high-molecular-weight perfluoroalkane barrier layers that might be useful in coating photocatalysts for technological reasons.

## II. Experimental Section

**A. Vacuum System and Photoreactor.** The stainless steel vacuum system is pumped simultaneously with a Pfeiffer Vacuum 60 L/s turbomolecular pump and a Varian 20 L/s ion pump. The system has a base pressure of $\sim 10^{-8}$ Torr, as measured by the ionization current within the ion pump. This base pressure is reached after 24 h baking of the system while pumping with both pumps. The pressure of reactant gases was measured with an MKS capacitance manometer (Baratron, type 116A, range $10^{-3}-10^{3}$ Torr).

The dual-beam IR−UV photoreactor used in these experiments has been described previously.[16,17] The stainless steel photoreactor can be used at pressures from $\sim 10^{-8}$ to $\sim 760$ Torr and at photocatalyst temperatures from 100 to 1500 K. The powdered $TiO_2-SiO_2$ sample is pressed hydraulically at 12 000 lbs/in$^2$ into the openings of a flat tungsten grid[18] (0.0508 mm thick, with 0.22-mm$^2$ square holes, obtained from Buckbee-Mears, St. Paul, MN). The grid is supported inside the dual-beam IR−UV photoreactor using Ni heating and cooling clamps along the grid edges. The grid is oriented at a 45° angle to both the IR and the UV beams so that the irradiation of the grid with UV light directed perpendicular to the IR beam can be carried out without making a geometrical change. A type-K thermocouple is spot welded to the top-center region of the grid. The sample is heated using the electrical resistance of the tungsten grid. The power leads and the type-K thermocouple leads pass through a re-entrant Dewar and connect to a power supply controlled by a Honeywell digital controller.[19] The cooling is realized by filling the Dewar with two different cooling agents: liquid $N_2$ or a mixture of dry ice−acetone. In the experiments carried out from 243−253 K, the cooling agent

* Corresponding author. E-mail: jyates@pitt.edu.

10.1021/jp031168k CCC: $27.50 
Published on Web 02/07/2004

was a dry ice−acetone mixture. The accuracy of the temperature control was ±2 K.

The cell is equipped with KBr infrared windows mounted on concentric Viton O-rings that are differentially pumped to prevent leaks. The IR−UV photoreactor is connected through a gas port to the ultrahigh vacuum system. The photoreactor is mounted on a computer-controlled translation system (Newport Corporation) with ±1-$\mu$m accuracy[16] in both the horizontal and vertical directions. This allows one to align different positions on the same grid with respect to the IR beam. The middle and the lower positions on the grid are used as sample spots. The upper position on the grid is empty and is used for the background absorbance measurements in the same experiment.

**B. Materials.** The $TiO_2-SiO_2$ sample was prepared in the laboratory of Professor K. Klabunde, Kansas State University, using a modified aerogel procedure, as reported previously.[14] This procedure[20] is applied to the production of different intimately intermingled mixed oxides, essentially molecular in nature. The advantage of this procedure is to obtain higher surface areas of the more reactive component throughout the structure, in this case $TiO_2$ (photoactive in nature) with $SiO_2$ (which supports very high surface areas). Thus, the $TiO_2-SiO_2$ mixed oxide (50 mol % $TiO_2$ and 50 mol % $SiO_2$) has very high surface area (680 $m^2/g$), a large pore volume (2.97 $cm^3/g$), and an average pore diameter (175 Å). The BET data for the pore-size distribution showed the presence of a substantial number of pores with diameters of ~10 Å.

The $SiO_2$ sample used as a reference adsorbent was Aerosil 200 obtained from Degussa. Its surface area was 200 $m^2/g$.

The samples are hydraulically pressed into the tungsten grid as a circular spot 7 mm in diameter, typically weighing 1−1.5 mg (1.3−1.9 $mg/cm^2$). The samples and the grid support assembly are then placed into the dual beam IR−UV photoreactor and evacuated.

The 2-chloroethyl ethyl sulfide (98%) used for this work was obtained from Aldrich, and the perfluorononane $C_9F_{20}$ (99%), from Lancaster Synthesis. These liquids were transferred under nitrogen gas to glass bulbs and purified by five freeze−pump−thaw cycles. The storage bulbs are attached to the stainless steel gas line, and the vapor is transferred to the dual-beam IR−UV photoreactor from the bulbs. The oxygen used was obtained from VWSCO and was 99.8% pure.

**C. Sample Activation and IR Measurement.** The $TiO_2-SiO_2$ sample was heated in vacuum to the desired pretreatment temperature at a rate of 20 K/min. Consecutive oxidation and thermal reduction procedures are applied for the initial activation of a fresh sample and for the reactivation of a used sample. The fresh sample was treated in vacuum at 675 K for 4 h and then treated with 6.2 Torr $O_2$ for 0.5 h at the same temperature. After 10 min evacuation, the sample was cooled to room temperature in vacuum, and the reference spectra for the oxidized sample were taken. After that, the sample was reduced in vacuum at 1026 K for 3 h and then cooled to room temperature, and the reference spectra for the thermally reduced sample were taken. The oxidation and the thermal treatments remove traces of residual organic species that could come from remnant alkoxy groups retained by the mixed oxide after the preparation procedure. The thermal treatment caused Ti−OH groups to be removed from the fresh sample, leaving only Si−OH groups behind.[10,14] The treatment at 1026 K caused an elevation of the background absorption across the IR spectrum due to the production of trapped electrons that interact with IR photons over a wide energy range.[21] The IR background absorption measured for the oxidized and the thermally reduced

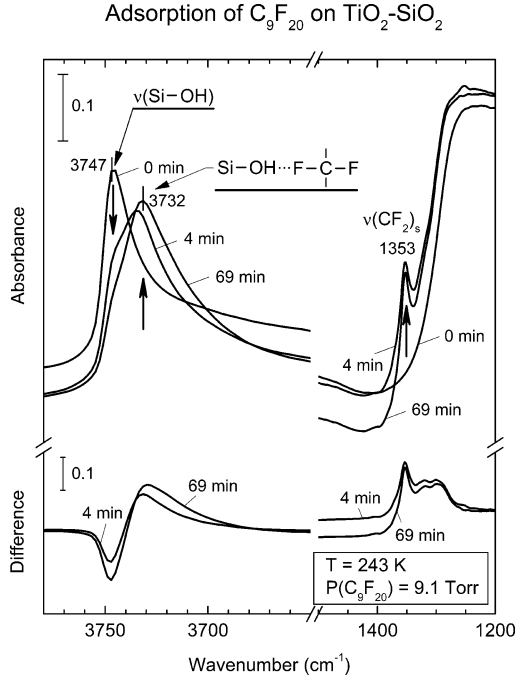


**Figure 1.** IR spectra for $C_9F_2$ adsorption on the $TiO_2-SiO_2$ photocatalyst powder. Both the actual spectra and difference spectra are shown in selected spectral regions. $T = 243$ K.

sample together with the intensity of the IR band due to Si−OH groups were used to characterize the state of the sample before each adsorption or photooxidation experiment. Because we employed the same sample for the whole set of experiments, we used the above oxidation and thermal reduction procedures to restore the $TiO_2-SiO_2$ surface to its initial state. For this purpose, the sample was evacuated at 675 K for 30 min, treated with 6.2 Torr $O_2$ for 30 min at the same temperature, and then reduced in vacuum at 1026 K for 10 min.

The IR spectra were measured with a nitrogen-gas-purged Mattson FTIR spectrometer (Research Series I) equipped with a liquid-$N_2$-cooled HgCdTe detector. All scans in the IR region from 4000 to 500 $cm^{-1}$ were made in the ratio mode at a resolution of 4 $cm^{-1}$. Typically, 200 scans were accumulated in each spectrum. The spectrometer was controlled from a personal computer using WinFIRST software supplied by Mattson.

**D. Adsorption and Photooxidation Experiments.** The adsorption of $C_9F_{20}$ was carried out on a thermally reduced $TiO_2-SiO_2$ sample at 243 K. The pressure of $C_9F_{20}$ admitted into the cell was 9.1 Torr, which is close to the equilibrium vapor pressure of 11.7 Torr $C_9F_{20}$ at 298 K (CAPLUS, Ref No. 375-96-2). To check for the completeness of $C_9F_{20}$ interaction with the $TiO_2-SiO_2$ sample, a second admission of the same pressure (9.1 Torr $C_9F_{20}$) was made. The observed increases in the absorbance for both characteristic IR features (hydrogen-bonded $\nu$(Si−OH) and $\nu(CF_2)_{as}$) were less than 5% of the absorbance produced during the first admission. This proved that little additional fluorocarbon can be adsorbed on the $TiO_2-SiO_2$ surface under the conditions employed.

The adsorption of 2-CEES on a clean and a $C_9F_{20}$ precovered surface was carried out at 243 K and at the 2-CEES vapor pressure of 0.160 Torr.

The adsorption of $O_2$ at two different pressures (0.160 and 20.7 Torr) was carried out at 253 K because the higher pressure of $O_2$ caused some warming of the grid containing the $TiO_2-SiO_2$ sample. The kinetics of oxygen interaction with trapped electrons in the bulk phase of the $TiO_2$-type regions of the

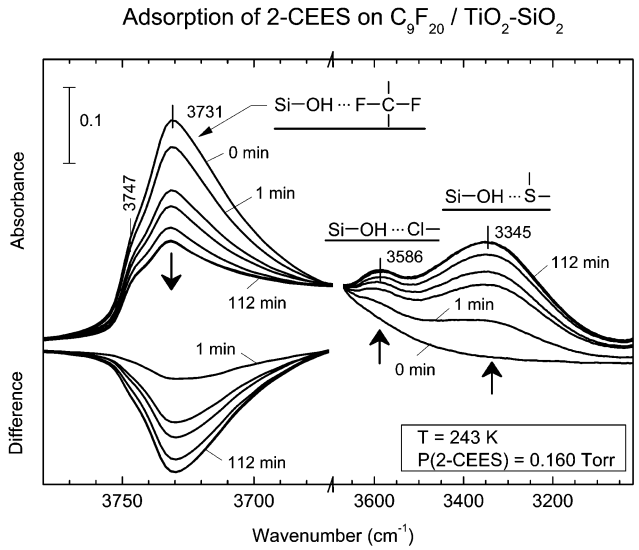


**Figure 2.** Spectral changes for 2-CEES adsorption on top of a thick $C_9F_{20}$ layer, preadsorbed. $T = 243$ K.

$TiO_2-SiO_2$ sample were used as a measure of the oxygen diffusion rates into clean, $C_9F_{20}$, and 2-CEES + $C_9F_{20}$ precovered surfaces.

The photooxidation experiments with $C_9F_{20}/TiO_2-SiO_2$ were carried out at 200 K, and that with 2-CEES/$C_9F_{20}/TiO_2-SiO_2$ and 2-CEES/$TiO_2-SiO_2$ at 253 K, in the presence of 20.7 Torr $O_2$.

A 350-W high-pressure Hg arc (Oriel Corp. 18) lamp is employed as a UV light source. The light was filtered with a water filter to remove the IR radiation and was focused onto the sample through a sapphire window. The intensity of the UV radiation on the sample was 240 mW/cm$^2$ in the energy range of 2.1−5 eV.

## III. Results

**A. Adsorption and Diffusion.** Figure 1 shows the spectral behavior observed for the adsorption of $C_9F_{20}$ on the $TiO_2-SiO_2$ mixed oxide photocatalyst surface. The gas was adsorbed in two doses at 9.1 Torr at 243 K to witness the slow diffusion of the molecule into the bulk of the mixed oxide. The fluoroalkane interacts with isolated Si−OH groups that exist throughout the catalyst depth,[14] causing a red shift for the Si−O−H stretching mode of about 15 cm$^{-1}$ from 3747 to 3732 cm$^{-1}$. It is observed that even after 69 min, when spectral changes have ceased to occur, only a fraction (∼50%, as approximated from the difference spectra) of the isolated Si−OH groups have become hydrogen bonded to $C_9F_{20}$ molecules. This is likely to be due to the presence of a fraction of the Si−OH groups in small pores that are unable to transport the large $C_9F_{20}$ molecule. The adsorption of $C_9F_{20}$ may also be monitored by observing the development of the 1353-cm$^{-1}$ feature due to the $\nu(CF_2)_s$ symmetric stretching motion.[22] Small background shifts due to $C_9F_{20}$ adsorption make a quantitative measurement of the intensity changes difficult in this spectral region. The difference spectra in the Si−OH region, as shown in the bottom part of Figure 1, are especially valuable in observing the process of hydrogen bonding of the perfluoroalkane to isolated Si−OH groups.

The admission of a second 9.1-Torr dose of $C_9F_{20}$ at 243 K caused only negligible additional changes in the absorbance for both IR features ($\nu$(Si−OH) and $\nu(CF_2)_s$, not shown here), which were less than 5% of those obtained during the first admission (Figure 1). This proved that $C_9F_{20}$ molecules from the gas phase cannot find more sites for adsorption on the $TiO_2-SiO_2$ surface (i.e., the formation of a thick $C_9F_{20}$ layer is complete).

It was of interest to study the adsorption of the 2-CEES molecule on top of the thick $C_9F_{20}$ layer to determine whether a 2-CEES layer would form on top of the $C_9F_{20}$ layer at 243 K.

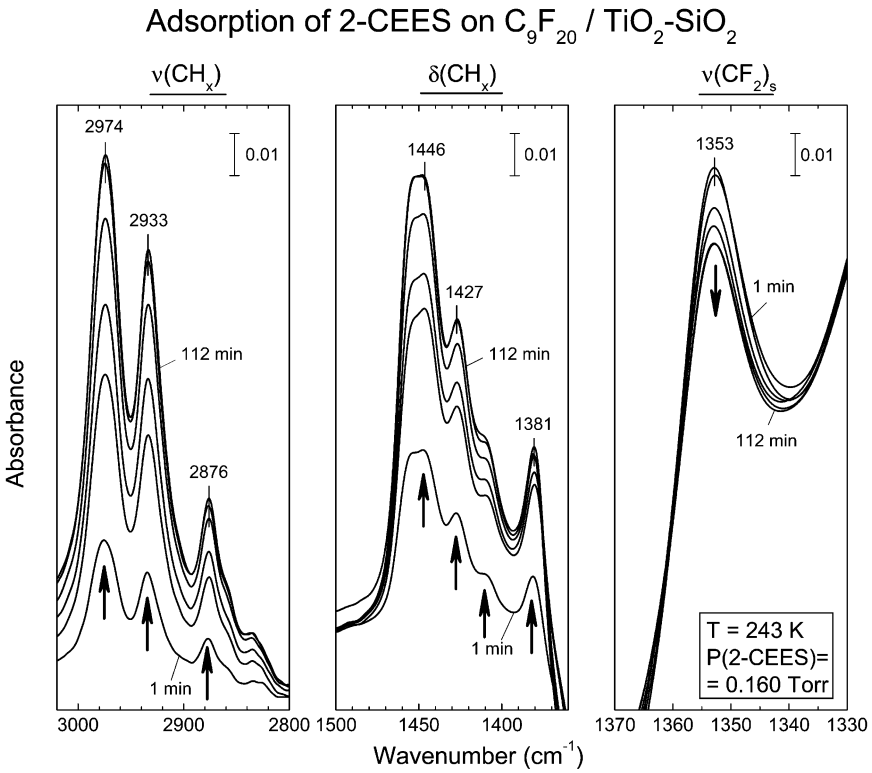


**Figure 3.** Spectral changes for 2-CEES adsorption on top of a thick $C_9F_{20}$ layer, preadsorbed. $T = 243$ K.

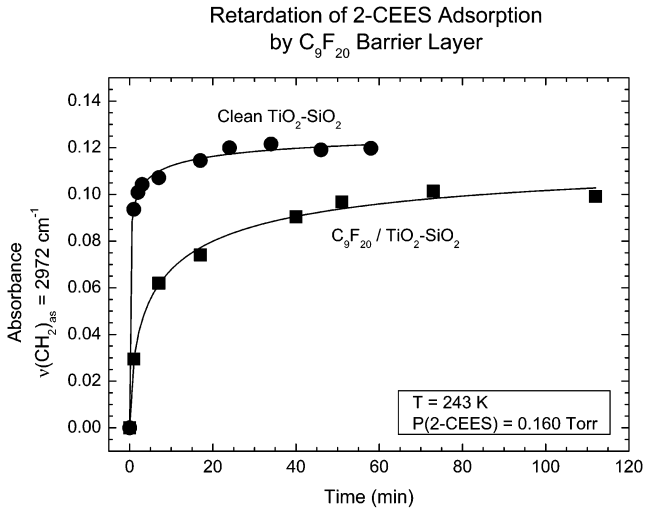


**Figure 4.** Kinetics of 2-CEES adsorption on a clean $TiO_2-SiO_2$ photocatalyst surface and on the same surface with a thick barrier layer of $C_9F_{20}$. $T = 243$ K.

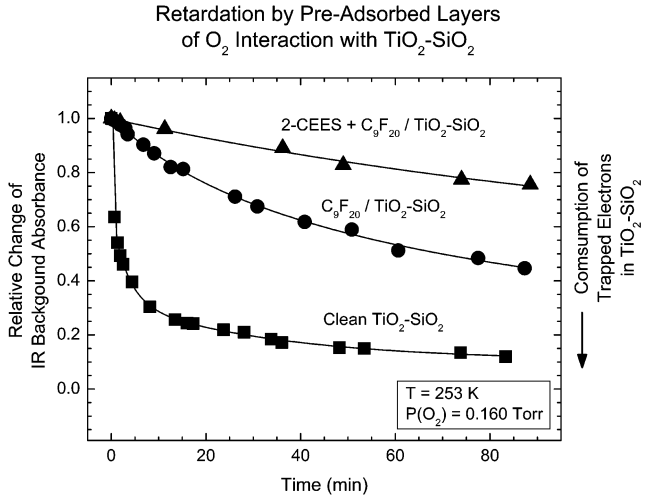


**Figure 5.** Retardation of $O_2$ adsorption by preadsorbed layers using the shift of the IR background absorbance at 2121 $cm^{-1}$. $T = 253$ K.

Figure 2 shows this experiment, and we see that both the free Si−OH mode at 3747 $cm^{-1}$ and the red-shifted mode at 3731 $cm^{-1}$ due to Si−OH hydrogen bonding to the perfluoroalkane are influenced by 2-CEES adsorption. The difference spectra in the OH region are particularly informative; associated with the loss of OH absorbance in the 3750−3700-$cm^{-1}$ region, more highly shifted Si−OH modes are observed to develop at 3586 and 3345 $cm^{-1}$. These two modes are due to hydrogen bonding to two moieties in the 2-CEES molecule—the Cl and the S molecular sites as previously reported[14]—as shown in Figure 2. This simple experiment indicates that the following effects are seen: (1) $C_9F_{20}$, hydrogen bonded to Si−OH groups, is displaced by 2-CEES, which bonds bifunctionally to Si−OH. (2) The 2-CEES molecule also finds Si−OH groups that are not accessible to $C_9F_{20}$ and bonds to these groups, causing a depletion of the intensity of unbonded Si−OH groups ($\nu$(Si−OH) = 3747 $cm^{-1}$) in the photocatalyst.

Figure 3 shows the growth of mode intensity in the $\nu(CH_x)$ stretching region and the $\delta(CH_x)$ deformation region due to 2-CEES adsorption on top of the $C_9F_{20}$ buffer layer. Spectral changes at 1353 $cm^{-1}$ indicate a slight reduction in the $\nu(CF_2)_s$ mode intensity due to the fractional displacement of $C_9F_{20}$.

Whereas the adsorption of 2-CEES readily occurs on the $C_9F_{20}$-covered photocatalyst, the kinetics of adsorption is

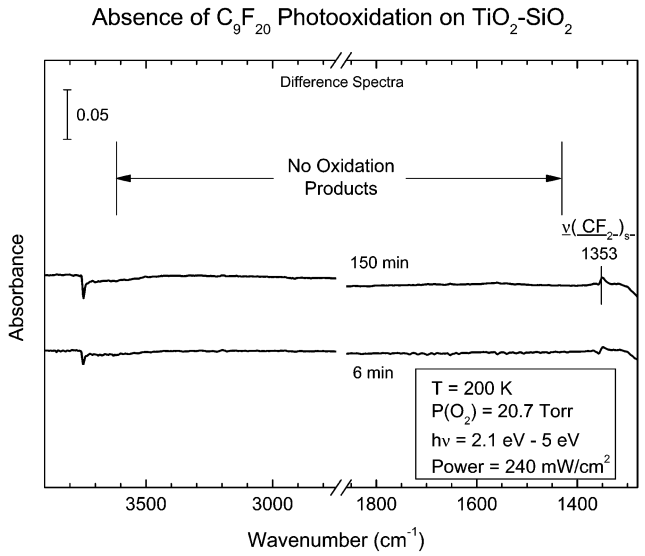


**Figure 6.** Control experiment showing that $C_9F_{20}$ is not photooxidized on $TiO_2-SiO_2$. $T = 200$ K.

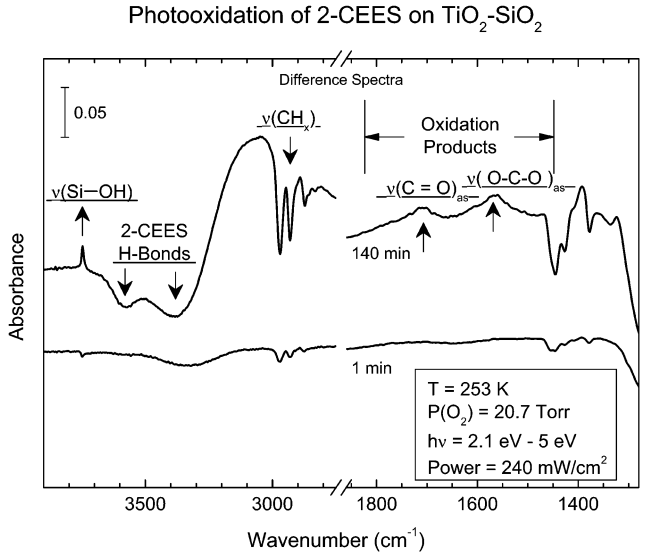


**Figure 7.** IR spectral changes during 2-CEES photooxidation on $TiO_2-SiO_2$. $T = 253$ K.

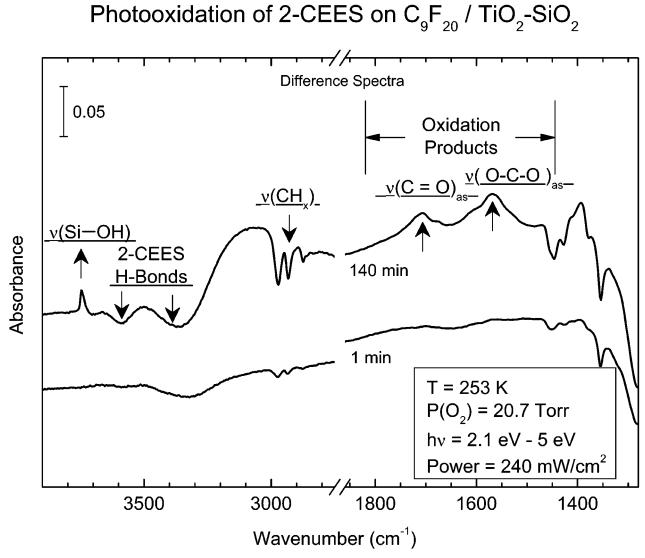


**Figure 8.** IR spectral changes during 2-CEES photooxidation on $TiO_2-SiO_2$ in the presence of a thick buffer layer of $C_9F_{20}$. $T = 253$ K.

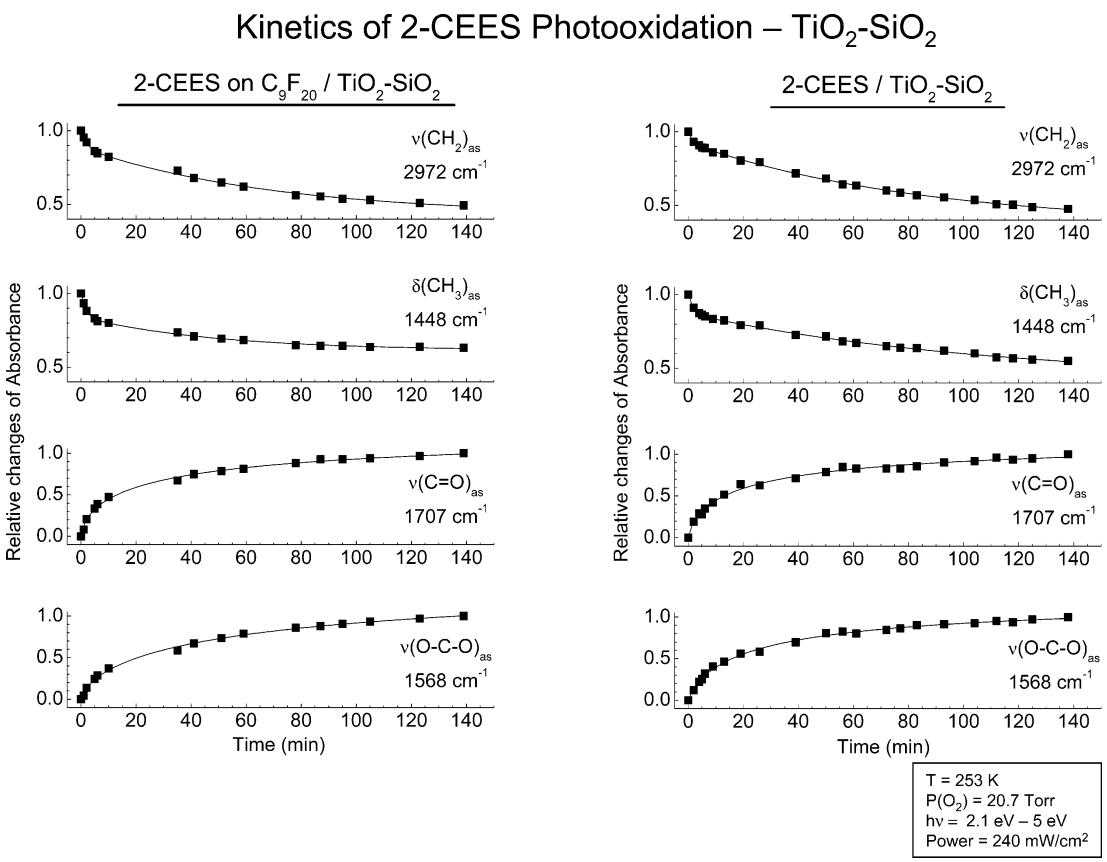


**Figure 9.** Comparison of the kinetics of photooxidation of 2-CEES with and without a $C_9F_{20}$ buffer layer. $T = 253$ K.

retarded by the perfluoroalkane overlayer. Figure 4 shows a comparative kinetic measurement under the same conditions of temperature, 2-CEES pressure, and using the same sample of $TiO_2-SiO_2$ powder. The rate of development of the $\nu(CH_2)_{as}$ mode intensity is somewhat retarded when the thick $C_9F_{20}$ layer is present.

The $TiO_2-SiO_2$ photocatalyst, as prepared by heating in vacuum, possesses oxygen vacancy defects that are associated with trapped electrons just below the conduction band. These electrons may be excited by IR photons into a continuum of states resulting in a broadband absorption of light, causing the elevation of the background across the IR spectrum.[21] This effect is therefore useful in two ways: (1) One can monitor the concentration of these defects and the associated trapped electrons. (2) One can monitor the bonding of molecular $O_2$ to the $TiO_2$ regions of the mixed oxide catalyst because this molecule (and other electrophilic molecules) will abstract these trapped electrons, causing the IR background to decrease in absorbance.[21] We have therefore used this effect to monitor $O_2$ penetration through the thick $C_9F_{20}$ layer and the mixed $C_9F_{20}$ + 2-CEES layer, as shown in Figure 5. The clean $TiO_2-SiO_2$ powder responds to a small pressure of $O_2$ through at least two rate processes, a fast process that culminates in a few minutes and a slow process occurring over 100 min or more. When either $C_9F_{20}$ or 2-CEES + $C_9F_{20}$ layers are present, the fast process is absent, and the adsorption of $O_2$ occurs only with slow kinetics. The mixed organic layer exhibits the slowest $O_2$ adsorption kinetics.

**B. Photooxidation Experiments.** *1. Control Studies of $C_9F_{20}$ under Photooxidation Conditions.* One of our goals was to determine whether the photooxidation of the 2-CEES molecule is impeded by the presence of the perfluoroalkane buffer layer. Therefore, the possibility that $C_9F_{20}$ itself could be photooxidized was investigated, as shown in Figure 6. It may be seen that although some loss of Si−OH intensity occurs after UV irradiation and small changes occur in the frequency of the $\nu(CF_2)_s$ mode because of the removal of hydrogen-bonding Si−OH groups, no vibrational frequencies due to the formation of either O−C−O groups or C═O groups develop. Thus, as expected, the perfluoroalkane is not photooxidized.

*2. Photooxidation of 2-CEES on the $TiO_2-SiO_2$ Photocatalyst.* Figure 7 shows difference spectra generated when a pure 2-CEES layer is photooxidized on the clean photocatalyst surface.

In irradiation periods from 1 to 140 min, losses and gains in IR intensity are observed as photooxidation occurs. Hydrogen-bonded $\nu$(Si−OH) vibrational modes associated with the 2-CEES molecule decrease in intensity as the 2-CEES molecule is destroyed, and free Si−OH species are regenerated. Modes associated with $CH_x$ motions in the 2-CEES molecule are diminished in absorbance as 2-CEES is photooxidized. Final oxidation products, containing carbonyl groups and carboxylate groups, are produced by photooxidation, as may be seen in the upper difference spectrum of Figure 7. These results are in accordance with previous results from this laboratory[10] and serve as a reference for studies of 2-CEES photooxidation in the presence of the $C_9F_{20}$ buffer layer.

Figure 8 shows photooxidation studies on the 2-CEES + $C_9F_{20}$ layer, where 2-CEES is adsorbed following the adsorption of a thick $C_9F_{20}$ layer at 243 K. The photooxidation experiment occurs at 253 K because of the increasing thermal conductivity of the high pressure of $O_2$ (20.7 Torr) and the radiation source. By comparing Figures 7 and 8, one can see that the changes in the spectra related to 2-CEES destruction are essentially identical in the two cases, indicating that the buffer layer of $C_9F_{20}$ does not interfere chemically with the photooxidation process.

The kinetic behavior of the photooxidation of the pure 2-CEES and the 2-CEES influenced by a thick layer of $C_9F_{20}$

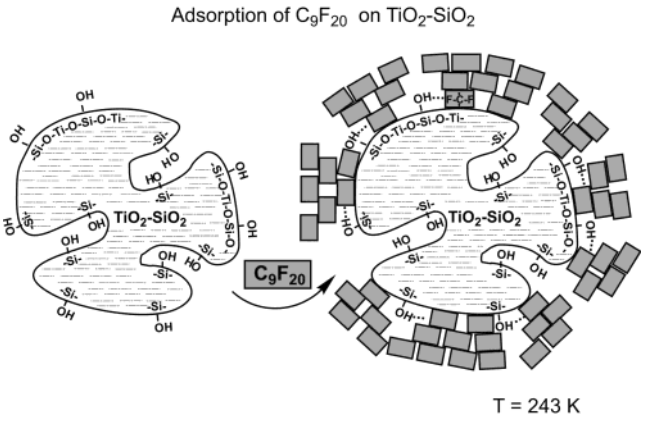


**Figure 10.** Schematic diagram of the adsorption of $C_9F_{20}$ on a porous $TiO_2-SiO_2$ photocatalyst. $T = 243$ K.

is compared in Figure 9. Both the kinetics of the destruction of 2-CEES and the production of the carbonyl- and carboxylate-containing oxidation products are compared, and it may be seen that the kinetics of oxidation is essentially similar in the two situations. The thick $C_9F_{20}$ buffer layer has little influence on the kinetics of 2-CEES photooxidation.

## IV. Discussion

The measurements given in this paper lead to a qualitative understanding of the photochemical behavior of $TiO_2-SiO_2$ photocatalyst material covered with a thick buffer layer of $C_9F_{20}$, maintained at a temperature slightly below its melting point. The results are best communicated by schematic diagrams showing the processes observed.

In Figure 10, the porous photocatalyst is schematically depicted. One sees outer sites containing separate $SiO_2$ and $TiO_2$ regions, which is consistent with our understanding of the phase separation between oxide phases that occurs when the mixed oxide is heated to 1026 K during its preparation and activation for photochemistry.[10,12,14,23,24] Only isolated Si−OH groups remain on the activated photocatalyst,[14] and these serve to hydrogen bond adsorbed $C_9F_{20}$ and 2-CEES molecules. We show two general classes of Si−OH groups—those on the outer surface of the nanoparticle mixed oxide and those within the pores. When a thick layer of $C_9F_{20}$ is adsorbed (Figure 1), a fraction of the isolated Si−OH groups are hydrogen bonded to $C_9F_{20}$, and a fraction are not influenced by the perfluoroalkane. We believe that Si−OH groups inside the small pores of the mixed oxide are sterically isolated from the large $C_9F_{20}$ molecules and remain uninfluenced by the thick buffer layer. This is schematically shown on the right-hand side of Figure 10 for the multilayer adsorption of $C_9F_{20}$.

Figure 11 schematically shows the behavior of the buffer layer of the perfluoroalkane-covered $TiO_2-SiO_2$ when 2-CEES is added, as deduced from the spectral behavior in Figure 2. First, it is clear that facile diffusion of 2-CEES occurs through the $C_9F_{20}$ buffer layer. Two separate effects are observed in the spectral developments in Figure 2: (1) Hydrogen-bonded $C_9F_{20}$ species are displaced by 2-CEES, which forms two types of stronger hydrogen bonds (Si−OH···Cl and Si−OH···S) judging from the Si−OH red shifts observed. (2) Isolated Si−OH groups, which were not hydrogen bonded to $C_9F_{20}$, become bonded to 2-CEES either through the S moiety or through the Cl moiety. It is likely that the smaller 2-CEES molecule can enter the pore structure of the $TiO_2-SiO_2$ photocatalyst, finding sites that were not influenced by preadsorbed $C_9F_{20}$ due to steric effects limiting the access of the large perfluorocarbon molecule to these sites.

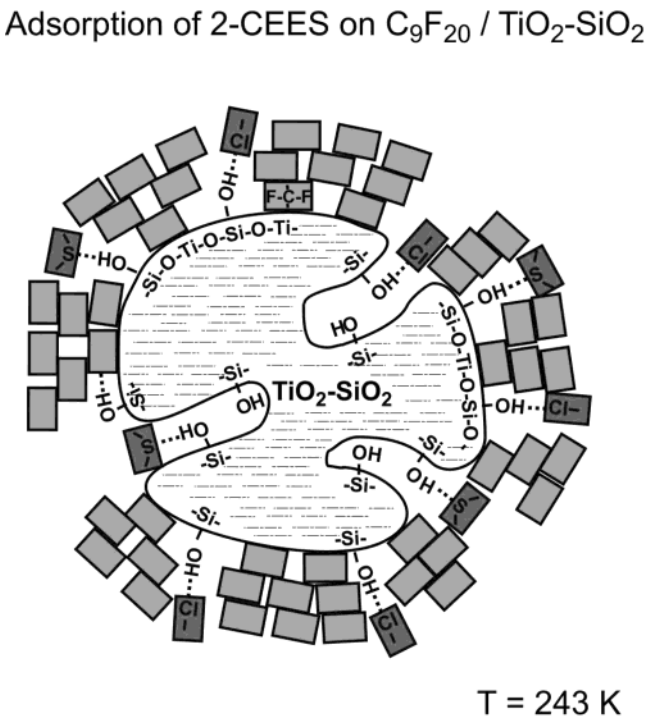


**Figure 11.** Schematic diagram of the adsorption of 2-CEES on top of a thick $C_9F_{20}$ buffer layer. $T = 243$ K.

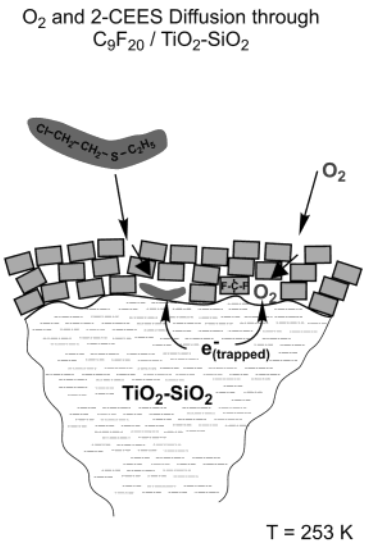


**Figure 12.** Schematic diagram of the diffusion of 2-CEES and $O_2$ through a thick layer of $C_9F_{20}$ at 243 K. Facile diffusion of both reactants provides access to the photocatalyst surface for adsorption, where photooxidation occurs without appreciable kinetic retardation compared to that for experiments in the absence of the perfluoroalkane buffer layer.

Figure 5 clearly shows that a thick buffer layer of $C_9F_{20}$ does not limit the access of molecular oxygen to the photocatalyst surface; only the adsorption kinetics change, and the fast $O_2$ adsorption process characteristic of the clean photocatalyst is replaced by a slower $O_2$ adsorption process. It is well known that fluorocarbons, such as FC 43, can be used for facile $O_2$ transport and production of a totally synthetic medium for the perfusion of an isolated rat brain,[25] and these results are consistent with this property.

Figure 12 schematically summarizes the observation of the facile diffusion of both 2-CEES and $O_2$ through the $C_9F_{20}$ buffer layer to the photoactive $TiO_2-SiO_2$ photocatalyst surface. The electrophilic $O_2$ molecule then abstracts trapped electrons from

the defective $SiO_2-TiO_2$ surface. From previous studies, we know that the Cl moiety in 2-CEES also imparts enough electrophilicity to the molecule to abstract trapped electrons from the photocatalyst,[21] and this process is schematically illustrated in Figure 12 also.

Under the influence of UV irradiation, our experiments demonstrate that the facile photooxidation of 2-CEES occurs under the $C_9F_{20}$ buffer layer, involving $O_2$ and 2-CEES reactant species that diffuse through the perfluoroalkane buffer layer and then bond to the photocatalyst surface.

The extension of these ideas to high-molecular-weight perfluorocarbon buffer films remains to be studied.

**Acknowledgment.** We acknowledge with thanks the support of this work by the DoD Multidisciplinary University Research Initiative (MURI) program administered by the Army Research Office under grant DAAD 19-01-0-0619. We also thank Professor K. Klabunde for supplying the $TiO_2-SiO_2$ photocatalyst powder and the characteristic BET data on surface area and pore-size distribution.

## References and Notes

(1) Fox, M. A.; Dulay, M. T. *Chem. Rev.* **1993**, *93*, 341.

(2) Hoffmann, M. R.; Martin, S. T.; Choi, W.; Bahnemann, D. W. *Chem. Rev.* **1995**, *95*, 69.

(3) Linsebigler, A. L.; Lu, G.; Yates, J. T., Jr. *Chem. Rev.* **1995**, *95*, 735.

(4) Mills, A.; Le Hunte, S. *J. Photochem. Photobiol., A* **1997**, *108*, 1−35.

(5) *Photocatalytic Purification and Treatment of Water and Air*; Ollis, D. F., Al-Ekabi, H., Eds.; Elsevier: Amsterdam, 1993.

(6) Fujishima, A.; Hashimoto, K.; Watanabe, T. *$TiO_2$ Photocatalysis: Fundamentals and Applications*; BKC: Tokyo, 1999.

(7) Vorontsov, A. V.; Savinov, E. V.; Davydov, L.; Smirniotis, P. G. *Appl. Catal. B: Environ.* **2001**, *32*, 11.

(8) Kozlov, D. V.; Vorontsov, A. V.; Smirniotis, P. G.; Savinov, E. V. *Appl. Catal., B* **2003**, *22*, 77.

(9) Martyanov, I. N.; Klabunde, K. J. *Environ. Sci. Technol.* **2003**, *37*, 3448.

(10) Panayotov, D. A.; Paul, D. K.; Yates, J. T., Jr. *J. Phys. Chem. B* **2003**, *107*, 10571.

(11) Anderson, C.; Bard, A. J. *J. Phys. Chem.* **1995**, *99*, 9882.

(12) Anderson, C.; Bard, A. J. *J. Phys. Chem. B* **1997**, *101*, 2611.

(13) Deng, Z.; Wang, J.; Zhang, Y.; Weng, Z.; Zhang, Z.; Zhou, B.; Shen, J.; Cheng, L. *Nanostruct. Mater.* **1999**, *11*, 1313.

(14) Panayotov, D.; Yates, J. T., Jr. *J. Phys. Chem. B* **2003**, *107*, 10560.

(15) Lancaster Synthesis, Individual Product Details, Catalog N 17363

(16) Mawhinney, D. B.; Rossin, J. A.; Gerhart, K.; Yates, J. T., Jr. *Langmuir* **1999**, *15*, 4617.

(17) Rusu, C. N.; Yates, J. T., Jr. *J. Phys. Chem. B* **2000**, *104*, 1729.

(18) Ballinger, T. H.; Wong, J. C. S.; Yates, J. T., Jr. *Langmuir* **1992**, *8*, 1676.

(19) Muha, R. J.; Gates, S. M.; Basu, P. *Rev. Sci. Instrum.* **1985**, *56*, 613.

(20) Carnes, C. L.; Kapoor, P. N.; Klabunde, K. J.; Bonevich, J. *Chem. Mater.* **2002**, *14*, 2922.

(21) Panayotov, D. A.; Yates, J. T., Jr. *Chem. Phys. Lett.* **2003**, *381*, 154.

(22) Schönherr, H.; Ringsdorf, H. *Langmuir* **1996**, *12*, 3891.

(23) Yang, J.; Ferreira, J. M. F.; Weng, W.; Tang, Y. *J. Colloid Interface Sci.* **1997**, *195*, 59.

(24) Song, C. F.; Lu, M. K.; Yang, P.; Xu, D.; Yuan, D. R. *Thin Solid Films* **2002**, *413*, 155.

(25) Dirks, B.; Krieglstein, J.; Lind, H. H.; Rieger, H.; Schütz, H. *J. Pharmacol. Methods* **1980**, *4*, 95.